



Decationized polyplexes as stable and safe carrier systems for improved biodistribution in systemic gene therapy

Luís Novo^{a,1}, Larissa Y. Rizzo^{b,1}, Susanne K. Golombek^b, George R. Dakwar^c, Bo Lou^a, Katrien Remaut^c, Enrico Mastrobattista^a, Cornelus F. van Nostrum^a, Wilhelm Jahnhen-Dechent^d, Fabian Kiessling^b, Kevin Braeckmans^{c,f}, Twan Lammers^{a,b,e}, Wim E. Hennink^{a,*}

^a Department of Pharmaceutics, Utrecht Institute for Pharmaceutical Sciences, Utrecht University, 3584 CG Utrecht, The Netherlands

^b Nanomedicines and Theranostics, Department for Experimental Molecular Imaging, University Hospital RWTH Aachen, Pauwelsstrasse 30, 52074 Aachen, Germany

^c Laboratory for General Biochemistry and Physical Pharmacy, Faculty of Pharmacy, Ghent University, Ghent Research Group on Nanomedicines, Harelbekestraat 72, 9000 Ghent, Belgium

^d Helmholtz Institute for Biomedical Engineering, Biointerface Laboratory, RWTH Aachen University, Aachen, Germany

^e Department of Targeted Therapeutics, MIRA Institute for Biomedical Technology and Technical Medicine, University of Twente, Enschede, The Netherlands

^f Centre for Nano- and Biophotonics, Ghent University, Harelbekestraat 72, 9000 Ghent, Belgium

ARTICLE INFO

Article history:

Received 9 June 2014

Accepted 30 August 2014

Available online 7 September 2014

Keywords:

Gene delivery

Polymer

Nanoparticle

Biocompatibility

Biodistribution

EPR

ABSTRACT

Many polycation-based gene delivery vectors show high transfection *in vitro*, but their cationic nature generally leads to significant toxicity and poor *in vivo* performance which significantly hampers their clinical applicability. Unlike conventional polycation-based systems, decationized polyplexes are based on hydrophilic and neutral polymers. They are obtained by a 3-step process: charge-driven condensation followed by disulfide crosslinking stabilization and finally polyplex decationization. They consist of a disulfide-crosslinked poly(hydroxypropyl methacrylamide) (pHPMA) core stably entrapping plasmid DNA (pDNA), surrounded by a shell of poly(ethylene glycol) (PEG). In the present paper the applicability of decationized polyplexes for systemic administration was evaluated. Cy5-labeled decationized polyplexes were evaluated for stability in plasma by fluorescence single particle tracking (fSPT), which technique showed stable size distribution for 48 h unlike its cationic counterpart. Upon the incubation of the polymers used for the formation of polyplexes with HUVEC cells, MTT assay showed excellent cytocompatibility of the neutral polymers. The safety was further demonstrated by a remarkable low teratogenicity and mortality activity of the polymers in a zebrafish assay, in great contrast with their cationic counterpart. Near infrared (NIR) dye-labeled polyplexes were evaluated for biodistribution and tumor accumulation by noninvasive optical imaging when administered systemically in tumor bearing mice. Decationized polyplexes exhibited an increased circulation time and higher tumor accumulation, when compared to their cationic precursors. Histology of tumors sections showed that decationized polyplexes induced reporter transgene expression *in vivo*. In conclusion, decationized polyplexes are a platform for safer polymeric vectors with improved biodistribution properties when systemically administered.

© 2014 Elsevier B.V. All rights reserved.

1. Introduction

Gene therapy has generated great interest to be used as a therapeutic tool to solve unmet medical needs [1,2] and relies on the development of safe and efficient vectors. Nonviral vectors, such as cationic polymers, lipids and peptides, have been investigated in depth because of their flexibility and easiness of preparation when compared to viral vectors [3–9].

Polyplexes are normally formed by adding an excess of polycations to pDNA to yield positively charged and small-sized polyplexes which can, however, lead to significant toxicity *in vivo* [10,11]. Toxicity of

polycation-based vectors was especially evident for the “first-generation” homopolymer systems. Upon intravenous administration, cationic polyplexes show great instability *in vivo*, since they interact with negatively charged blood components (e.g. proteins, erythrocytes), followed by the formation of aggregates, leading to severe *in vivo* toxicity (lung embolism and/or liver necrosis) and uncontrollable biodistribution and off-targeting transfection [10–12]. Furthermore, cationic polymers/dendrimers might induce immunogenicity, complement activation and even blood coagulation [12–14].

Several strategies have been proposed and investigated to improve the *in vivo* behavior of polyplexes. Coating of polycation-based systems with PEG, effectively avoids the formation of aggregates and reduces protein binding, resulting in improvements of the circulation kinetics and tumor accumulation *in vivo* [12,15,16]. Another strategy to improve polyplex stability consists of the incorporation of disulfide crosslinks

* Corresponding author. Tel.: +31 30 253 6964; fax: +31 30 251 7839.

E-mail address: w.e.hennink@uu.nl (W.E. Hennink).

¹ Authors contributed equally to this work.

into the polyplex core. Disulfide crosslinks stabilize the polyplex structure in the bloodstream, avoiding unwanted disassembly in circulation, but these bonds can be rapidly cleaved in the intracellular reducing milieu [17–19]. *In vivo*, introduction of disulfide crosslinks, has demonstrated to improve circulation kinetics [20], as well as to improve tumor accumulation and transfection upon systemic administration [21]. However, further improvements on the blood circulation kinetics and biodistribution are of utmost importance to achieve the desired selective accumulation into target tissues. Even when shielded with PEG, the cationic groups of conventional polyplexes can also lead to unspecific cell binding in highly vascularized organs and, consequently, to poor *in vivo* biodistribution and insufficient blood circulation half-life [22,23].

The major challenge for the clinical applicability of polymeric vectors is to achieve therapeutic efficacy with minimal toxicity and side effects upon systemic administration. Toxicity arising from polycations occurs not only on the systemic level but also at the cellular basis. Introduction of biodegradability into cationic polymers leads to the development of safer systems [5,24]. However, during the development of new gene delivery polymer, toxicity is measured with cell viability assays in limited concentrations and exposure times, likely leading to underestimation of the toxicity problem. Toxicity is a complex process and requires deeper analysis at both acute and long term basis. When cationic polyplexes are taken up by cells, they will firstly compromise the cell membrane integrity [25–27]. Polycations can also disrupt the cell homeostasis by interaction with cellular polyanions (e.g. cell receptors, enzymes, mRNA or genomic DNA) [28]. Polycations can change the genomic expression profile [29–31] and induce the activation of oncogenes or even apoptosis [26,32]. Such consequences are directly related to the polycationic nature of synthetic vectors and have a substantial impact on the safety of such systems. Accordingly, neutral polymer based systems are a logical step to obtain not only to improve blood circulation kinetics and biodistribution but also to accomplish the necessary safety requirements.

In the previous work the development of decationized polyplexes was reported [33,34]. These polyplexes constitute of a core of disulfide-crosslinked pHPMA, surrounded by a PEG shell. Complexation with DNA to form polyplexes occurs by the transient presence of cationic charge in the core of the polyplexes. After structure stabilization by inter-chain disulfide crosslinking, the cationic groups are removed by hydrolysis, leading to a disulfide crosslinked polyplex based on a neutral polymer. As a result, entrapment of pDNA is exclusively based on disulfide crosslinks, providing an intracellularly triggered release mechanism. This means that pDNA release from decationized polyplexes occurs exclusively in a reducing environment, such as the intracellular milieu [17–19]. Importantly, the decationized polyplexes, in contrast to their cationic precursor, showed a low degree of nonspecific uptake, which is thought to be an important advantage for improved blood circulation and higher target tissue accumulation exploiting the enhanced permeation and retention (EPR) effect [35].

In this study, we evaluated the stability, safety and *in vivo* biodistribution as well as the ability of decationized polyplexes for tumor targeting applications. The stability in biological fluids was evaluated by fSPT [36], as well as the safety by the teratogenicity and mortality potential in zebrafish embryo assay in parallel with cytotoxicity tests *in vitro* [37], and biodistribution and tumor accumulation in a A431 tumor-bearing mice by noninvasive optical imaging based on the combination micro-computed tomography (μ CT) and fluorescence molecular tomography (FMT) [38]. Finally, transgene expression was also assessed by histological analysis of tumor cryosections.

2. Materials and methods

2.1. Materials

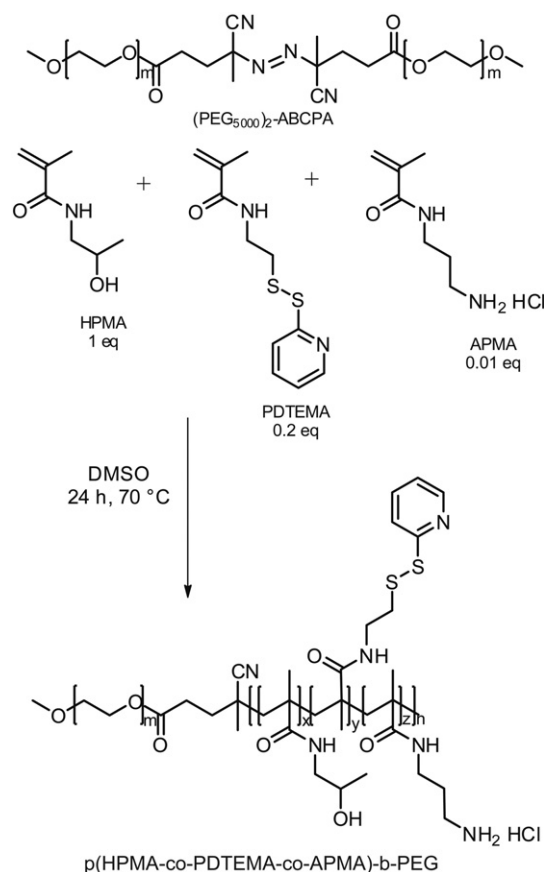
N-hydroxysuccinimide (NHS) ester functionalized dyes Cyanine5 NHS ester (Cy5-NHS) and Cyanine7 NHS ester (Cy7-NHS) were

obtained from Lumiprobe (Hannover, Germany). Carbonyldiimidazole (CDI) activation of *N,N'*-dimethylaminoethanol (DMAE) was performed as previously described to yield DMAE-Cl [39]. N-[2-(2-pyridyldithio)] ethyl methacrylamide (PDTEMA) was synthesized as previously described [33]. N-(3-aminopropyl)methacrylamide hydrochloride (APMA) was obtained from Polysciences (Eppelheim, Germany). The synthesis and characterization of (mPEG)₂-ABCPA (4,4'-azobis(4-cyanovaleric acid)) macroinitiator were done as previously described [40,41]. 2,4,6-Trinitrobenzene sulfonic acid (TNBSA) was obtained from ThermoScientific (Etten-Leur, The Netherlands). pCMV_EGFP plasmid, encoding for enhanced green fluorescent protein (EGFP) with human cytomegalovirus promoter (CMV), was amplified with competent *Escherichia coli* DH5 α and purified with NucleoBond® (Macherey-Nagel, Bioke, Leiden, The Netherlands). pCMV_EGFP construction was described by van Gaal et al. [42]. MTT Cell Proliferation Kit (3-(4,5-dimethylthiazol-2-yl)-2,5-diphenyl tetrazolium bromide) was purchased from Roche (Basel, Switzerland). Zebrafish medium was prepared in-house [37]. All other chemicals and reagents were obtained from Sigma-Aldrich (Zwijndrecht, The Netherlands). The following buffer systems were used: 4-(2-hydroxyethyl)-1-piperazineethanesulfonic acid (HEPES) for buffering at pH 6.8–8.2; 3-[[1,3-dihydroxy-2-(hydroxymethyl)propan-2-yl] amino]propane-1-sulfonic acid (TAPS) for buffering at pH 7.7–9.1.

2.2. Polymer synthesis

2.2.1. Synthesis of p(HPMA-co-PDTEMA-co-APMA)-b-PEG

Free radical polymerization using 5 kDa PEG bi-functionalized azo macroinitiator (PEG)₂-ABCPA was performed to synthesize p(HPMA-co-PDTEMA-co-APMA)-b-PEG (Scheme 1). The polymers were synthesized using a monomer to initiator ratio (M/I) of 220 (mol/mol). The



Scheme 1. Synthesis of p(HPMA-co-PDTEMA-co-APMA)-b-PEG, by free-radical polymerization of HPMA, PDTEMA and APMA using ((mPEG)₅₀₀₀)₂-ABCPA macroinitiator.

feed ratio HPMA/PDTEMA/APMA was 1/0.2/0.01 (mol/mol/mol). The polymerization was carried at 70 °C for 24 h in DMSO under an N₂ atmosphere, using 5 μmol macroinitiator and a monomer concentration of 0.4 M. After polymerization, the obtained product was precipitated in diethyl ether and collected by centrifugation. After removing ether under vacuum, the product was dissolved in 2.5 mM NH₄OAc pH 5 buffer and dialyzed for 2 days at 4 °C (MWCO 6000–8000 Da) against the same buffer. Finally, the product was collected by freeze-drying.

Unreacted PEG was removed by precipitation in cold EtOH (5 mg/mL of solids) followed by centrifugation and filtration over a 0.2 μm filter. The product, solubilized in EtOH, was collected after EtOH evaporation, dissolution in water and freeze-drying.

2.2.2. Synthesis of p(HPMA-DMAE-co-PDTEMA-co-Cy5/Cy7)-b-PEG

Firstly, a solution of p(HPMA-co-PDTEMA-co-APMA)-b-PEG · TFA ($M_w = 44.1$ kDa; 10 mg, 46.75 nmol NH₂/mg polymer, 1 eq.) was prepared in 100 μL of DMSO. Next, the polymer solution was slowly added to a 0.01 M Cy7-NHS or Cy5-NHS solution in 93.5 μL of DMSO (935 nmol, 2 eq.), containing 2.3 μmol (5 eq.) of triethylamine (Scheme 2). The reaction was performed for 36 h (in the dark) under stirring and N₂ atmosphere.

To determine the coupling efficiency, the crude product was diluted to a final polymer concentration of 1 mg/mL in DMF containing 10 mM LiCl and analyzed by GPC equipped with a UV detector set at 646 nm for

Cy5 and 700 nm for Cy7 detection. The coupling efficiency was determined by analyzing the area under the curve (AUC) of the polymer and unreacted dye peaks. AUC was determined using GraphPad Prism 5 (GraphPad Software Inc., La Jolla, California, USA).

A 1 M of DMAE-Cl solution in DMSO (451.5 μmol), corresponding to a 10-fold excess to HPMA reactive groups of the polymer, was added to the reaction mixture. The reaction was performed at room temperature for 24 h, in the dark and N₂ atmosphere to yield p(HPMA-DMAE-co-PDTEMA-co-Cy5/Cy7)-b-PEG (Scheme 2). After completion of the reaction, 1 M of acetic acid was added to adjust the pH 5. Removal of free dye was performed by dialysis against a mixture of EtOH/water 10 mM NH₄Ac pH 5 (50/50) for 2 days. The polymer was collected by freeze-drying after buffer exchange to 5 mM NH₄Ac pH 5 and desalting using PD-10 (GE Healthcare Life Sciences) columns following supplier's protocol.

2.2.3. Preparation of p(HPMA-co-PDTEMA)-b-PEG

To prepare p(HPMA-co-PDTEMA)-b-PEG (pHP-PEG), 5 mg of p(HPMA-DMAE-co-PDTEMA)-b-PEG (pHDP-PEG) was dissolved in 2.5 mL 10 mM HEPES 10 mM TAPS pH 8.5 buffer and hydrolyzed for 6 h at 37 °C. After hydrolysis the polymer was purified with a PD-10 column following supplier's protocol and collected by freeze-drying.

2.3. ¹H NMR characterization of the polymers

The composition of the polymers was determined by ¹H NMR analysis performed with a 400 MHz Agilent 400-MR NMR spectrometer (Agilent Technologies, Santa Clara, USA) in DMSO-d₆. The ratio HPMA/PDTEMA was determined by comparison of the integrals at δ4.6 ppm (bs, CH₂CHCH₃O, HPMA) and the integral at δ8.5 ppm (bs, pyridyl group proton, PDTEMA) ($\int \delta_{4.6} / \int \delta_{8.5}$). The integral ratios between δ4.2 ppm (bs, OCH₂CH₂), HPMA-DMAE) and δ4.6 ppm (bs, CH₂CHCH₃O, HPMA-DMAE) were used to verify reaction between DMAE-Cl and hydroxyl groups in the polymer from HPMA.

The number average molecular weight (M_n) of the polymers was determined according to Eq. (1).

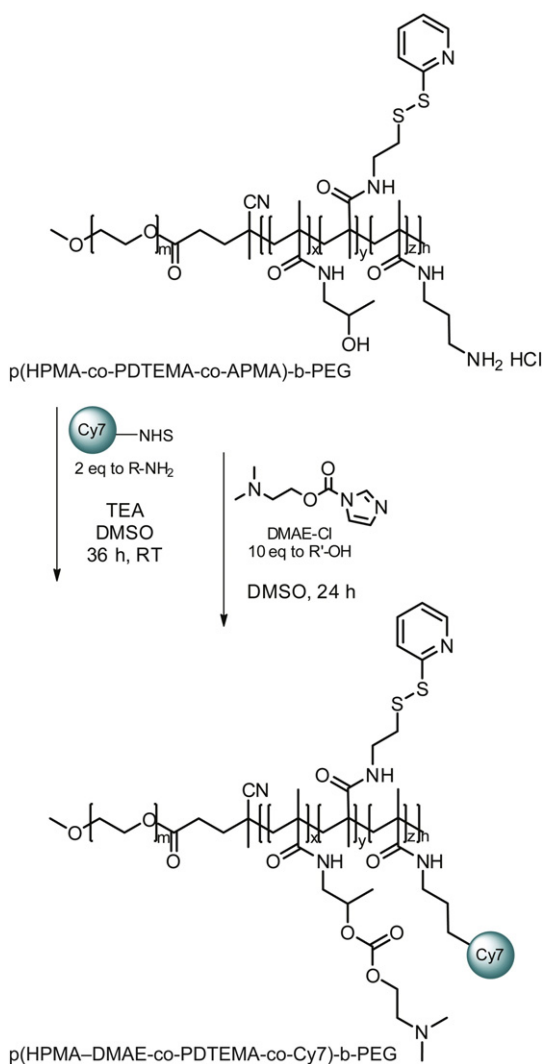
$$M_n = \left(\int \delta_{4.6} \times M_{(\text{HPMA}/\text{HPMA-DMAE})} + \int \delta_{8.5} \times M_{\text{PDTEMA}} \right) / \left(\int \delta_{3.5} / 448 \right) + 5000 \text{ (g/mol)} \quad (1)$$

where, $\int \delta_{3.5}$, $\int \delta_{4.6}$ and $\int \delta_{8.5}$ are the integrals at 3.5, 4.6, and 8.5 ppm, respectively. M_{HPMA} , $M_{\text{HPMA-DMAE}}$ and M_{PDTEMA} are the molar masses of HPMA, HPMA-DMAE and PDTEMA, respectively. The number of protons for the 5000 Da PEG block, at $\int \delta_{3.5}$, was set at 448.

2.4. UV spectroscopy characterization of the polymers

UV spectroscopy was performed on a Shimadzu UV-2450 UV/vis spectrophotometer (s-Hertogenbosch, The Netherlands) to quantify the molarity of thiol reactive pyridyl disulfide (PDS) groups per weight of polymer. Polymer stock solutions of 1 mg/mL were prepared in 20 mM HEPES pH 7.4 containing 50 mM of tris(2-carboxyethyl)phosphine (TCEP). After incubation for 1 h at 37 °C the UV absorbance at 343 nm was measured to determine the released 2-mercaptopyridine (2-MP) [43]. Quantification was performed using a calibration curve with 2-MP standards.

To quantify the molarity of dye Cy7 or Cy5 per weight of polymer, polymer stocks of 1 mg/mL in DMSO were prepared and the UV absorbance was measured at 646 nm for pHDP-Cy5-PEG or 750 nm for pHDP-Cy7-PEG. The quantification was done using a calibration curve of dye standards in DMSO.



Scheme 2. Synthesis of p(HPMA-DMAE-co-PDTEMA-co-Cy7)-b-PEG, by sequential coupling of Cy7-NHS and DMAE-Cl to p(HPMA-co-PDTEMA-co-APMA)-b-PEG.

2.5. TNBSA assay

In order to determine the molarity of free primary amines in p(HPMA-co-PDTEMA-co-APMA)-b-PEG, the TNBSA assay was performed [44]. Polymer solutions were prepared at 1 mg/mL in 0.1 M sodium bicarbonate buffer (pH 8.5) using glycine standards. The amine content was determined by detecting the absorbance at 420 nm.

2.6. Gel permeation chromatography (GPC) characterization of the polymers

GPC analysis of the polymers was performed using a Waters System (Waters Associates Inc., Milford, MA) with refractive index (RI) and UV detector using two serial Plgel 5 μ m MIXED-D columns (Polymer Laboratories) and DMF containing 10 mM LiCl as eluent. The flow rate was 1 mL/min (30 min run time) and the temperature was 60 °C. The average molecular weight (M_n), weight average molecular weight (M_w) and polydispersity (PDI, M_w/M_n) were determined by calibration with a series PEG calibration standards of different molecular weights and with narrow molecular weight distribution.

2.7. Preparation of decationized polyplexes

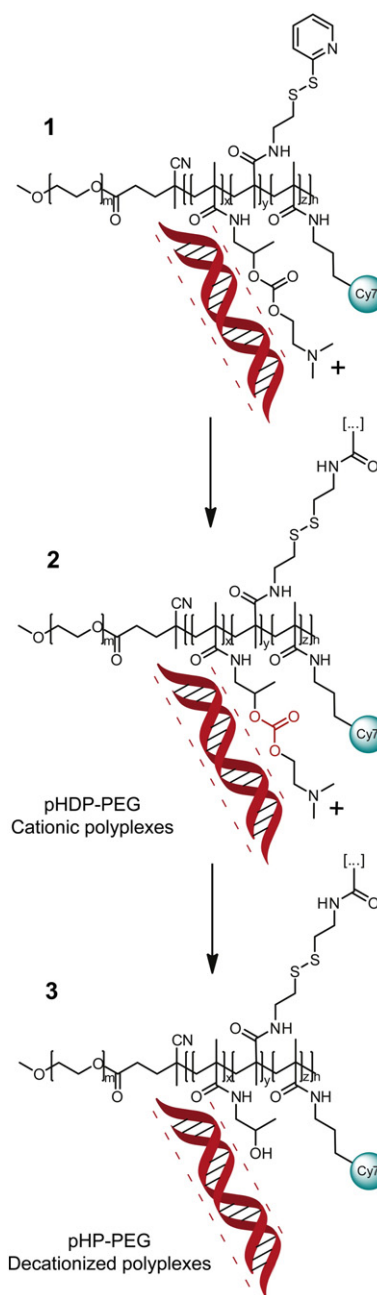
The preparation of Cy5/Cy7-labeled decationized polyplexes was adapted from the method previously described (Scheme 3) [33]. In order to prepare a high concentrated polyplex dispersion 400 μ g/mL pDNA, 80 μ L of aqueous solution of pHDP-PEG was mixed with 160 μ L of pDNA (pCMV_EGFP) (600 μ g/mL) in 10 mM HEPES 10 mM TAPS pH 8.5 buffer containing 5% glucose. The amount of polymer added to the pDNA solution corresponded to N/P = 4 (N, molarity of positively charged amines from polymer; P, molarity of negatively charged phosphates from pDNA). Subsequently, the formed polyplexes were crosslinked by the addition of dithiothreitol (DTT) corresponding with a half molar equivalent to PDS groups of the polymer, in order to induce self-crosslinking of the polyplexes [45] for 1 h at pH 8.5 at room temperature.

To prepare decationized pHDP-PEG polyplexes, the cationic DMAE side groups were removed by hydrolysis by the incubation of the polyplex dispersions at 37 °C in 10 mM HEPES 10 mM TAPS, pH 8.5 for 6 h [33]. Next, the pH of the dispersion was adjusted to pH 7.4. For cationic pHDP-PEG polyplexes the pH was adjusted to pH 7.4 immediately after the completion of the crosslinking step. When polyplexes needed to be stored for long periods, the pH of the dispersions was adjusted to pH 5 and the dispersions were stored at 0–5 °C, with the pH being readjusted to pH 7.4 immediately before use. Comparative studies were always performed by dividing the same batch of polyplexes into pHDP-PEG cationic and pHDP-PEG decationized polyplexes. Given the fact that the side products from cross-linking and decationization (2-mercaptopyridine and DMAE) have a high cellular tolerance [33,45,46], the polyplexes were directly used without purification procedures.

2.8. Particle size and zeta potential determination

The size of the polyplexes was measured with DLS on an ALV CGS-3 system (Malvern Instruments, Malvern, UK) equipped with a JDS Uniphase 22 mW He–Ne laser operating at 632.8 nm, an optical fiber-based detector, a digital LV/LSE-5003 correlator with temperature controller set at 25 °C or 37 °C. Measurements were performed in HBS (20 mM HEPES, 150 mM NaCl, pH 7.4) at a pDNA concentration of 40 μ g/mL.

Size distribution and polydispersity of the polyplexes were also determined by nanoparticle tracking analysis (NTA) measurements on a NanoSight LM10SH (NanoSight, Amesbury, United Kingdom), equipped with a sample chamber with a 532-nm laser. Polyplexes were diluted in phosphate buffered saline (PBS) to a concentration of 0.1 μ g/mL pDNA and measured for 160 s with manual shutter and gain adjustments. The captured videos were analyzed by the NTA 2.0 image analysis



Scheme 3. Route for the preparation of interchain disulfide-crosslinked decationized polyplexes, through a 3-step process: 1. charge-driven condensation with nucleic acids; 2. stabilization through disulfide crosslinking; 3. decationization of cationic pHDP-PEG polyplexes, resulting in decationized pHDP-PEG polyplexes (adapted from [33]).

software (NanoSight, Amesbury, UK). The detection threshold was set to 2 and the minimum track length to 10. The mode and mean size and SD values were obtained by the NTA software.

The zeta potential (ζ) of the polyplexes was measured using a Malvern Zetasizer Nano-Z (Malvern Instruments, Malvern, UK) with universal ZEN 1002 'dip' cells and DTS (Nano) software (version 4.20) at 25 °C. Zeta potential measurements were performed in 20 mM HEPES pH 7.4 at a pDNA concentration of 10 μ g/mL.

2.9. Stability using fluorescence single particle tracking (fSPT)

fSPT was performed to measure the stability of the cationic pHDP-PEG polyplexes and decationized pHDP-PEG polyplexes in full human

plasma. fSPT is a fluorescence microscopy technique that uses wide-field and a fast and sensitive CCD camera to record movies of diffusing particles in biofluids. These movies are analyzed using in-house developed software, to obtain size distributions as previously described [36].

fSPT measurements were performed as follows: a volume of 5 μL of sample of Cy5-labeled polyplex dispersion in HEPES buffer (20 mM pH 7.4) or in fresh plasma (10 $\mu\text{g}/\text{mL}$ final pDNA concentration) was placed between a microscope slide and cover glass with double-sided adhesive sticker, following incubation for different time points at 37 °C. Both the objective and the sample were kept at 37 °C during the measurements using an objective heater (Biophtechs, Butler, USA) and a sample heater (Linkam, Surrey, U.K.). Videos were recorded with the NIS Elements software (Nikon) driving the EMCCD camera (Cascade II:512, Roper Scientific, AZ, USA) and a TE2000 inverted microscope equipped with a 100 \times NA1.4 oil immersion lens (Nikon). To convert SPT diffusion measurements to size distributions, the viscosity of human plasma at 37 °C was set to 1.35 cP [36]. Human plasma was obtained from a healthy donor at UMC Utrecht. Blood was collected in EDTA tubes which were cooled on ice and subsequently centrifuged at 4 °C, 2000 $\times g$ for 10 min and plasma was isolated and stored at -80 °C.

2.10. Cell culture

HUVEC (human umbilical vein endothelial) cells were obtained from human umbilical cords and cultured in Endopan 3 (E3) medium (Pan Biotech, Germany), supplemented with 1% penicillin/streptomycin. A431 epidermoid carcinoma cells (ATCC) were cultured in Dulbecco's modified Eagle's Medium (DMEM; Gibco, Invitrogen, Germany), supplemented with 10% fetal bovine serum (FBS) (Invitrogen, Germany) and with 1% penicillin/streptomycin. Cell lines were kept at 37 °C and 5% CO_2 in a humidified atmosphere.

2.11. MTT assay

The cell viability upon incubation with decationized pHP-PEG and cationic pHDP-PEG polymers was evaluated via MTT assay, which measures the cellular metabolic activity of the cells. HUVECs were seeded into 96-well plates: 12,000 cells were seeded per well for 24 h test and 1950 cells per well were seeded for the 72 h test. After 24 h, the medium was refreshed and 30 μL of polymer samples in PBS was added to each well corresponding to a final concentration of 0.01–3 mg/mL also containing 12% FBS. After 24 h or 72 h, the MTT assay (Roche) was performed according to manufacturer's protocol. First, cells were washed with 200 μL PBS and 100 μL of cell culture medium was added per well. Next, MTT labeling reagent was added to a final concentration of 0.5 mg/mL. After 4 h at 37 °C and 5% CO_2 , the medium was discarded and 100 μL of DMSO was added per well to dissolve the formed formazan crystals. The plate was protected from light and formazan crystals were dissolved overnight at room temperature. The supernatants (100 μL) were then transferred into another 96-well plate and the absorbance was measured at 570 nm using reference wavelength of 690 nm.

2.12. In vivo toxicity using the zebrafish embryo assay

The *in vivo* toxicity of decationized pHP-PEG and cationic pHDP-PEG polymers was evaluated using the zebrafish (*Danio rerio*) embryo assay based on the method previously described in detail by Rizzo et al. [37]. In short, fertilized eggs were transferred into round-bottom 96-well plates (16-cell stadium, 1 egg per well). Polymers were diluted in fish medium corresponding to polymer concentrations ranging from 0.1 to 3 mg/mL. As positive control, branched polyethylenimine (b-PEI) 25 kDa was tested at 0.1 mg/mL. The development and survival of the

zebrafish embryos was evaluated for 72 h every 24 h post-fertilization using a Leica DMI 6000B inverted microscope.

2.13. Animal experiments

CD-1 nude female mice were fed with chlorophyll-free food pellets and water *ad libitum*. Mice were housed in ventilated cages and clinically controlled rooms and atmosphere. CD-1 nude mice were inoculated with A431 tumor cells (4×10^6 cells/100 μL) subcutaneously into the left flank 15 days before experiment, which lead to the development of A431 tumor xenografts with an approximate size of 6–7 mm in width.

Decationized pHP-PEG polyplexes (group 1, $n = 3$ and cationic pHDP-PEG polyplexes (group 2, $n = 3$) were tested for their *in vivo* biodistribution and tumor accumulation. Polyplex dispersions labeled with Cy7 were injected (80 μL , 32 μg pDNA, 2.5 nmol Cy7) into mice via tail vein under anesthesia. Immediately after sample injection, μCT (Tomoscope DUO; CT Imaging, Erlangen, Germany) and 3D FMT imaging (FMT2500; PerkinElmer), were performed essentially as previously described [38]. Briefly, mice were placed in a multi-modal imaging cassette under anesthesia (2% of isoflurane) to be firstly scanned in a μCT . Images with an isotropic voxel size of 35 μm were reconstructed using a modified Feldkamp algorithm with a smooth kernel. Immediately after μCT procedure, the animals were placed into the FMT docking station under 2% isoflurane anesthesia. The excitation wavelength channel was set to 750 nm. Whole body images of the mice were captured using FRI to allow the definition of the region of interest (ROI) and 3D scans were performed. μCT and 3D FMT images were collected 15 min, 4 h, 24 h and 48 h post-injection.

The obtained μCT and FMT scans were fused. Based on the μCT data, liver, kidneys, lungs, heart, bladder and tumor were segmented, using an Imalytics Research Workstation software (Philips Technologie GmbH Innovative Technologies, Aachen, Germany). FMT reconstructed signals were overlapped onto respective organ-segmented μCT images, and the amount accumulated Cy7 in these organs was quantified. The percentage injected dose (% ID) was calculated based on the quantification obtained for each segmented organ and normalized to the organ volume. In parallel to the imaging protocol, blood and urine samples were also collected at relevant time 2 min, 15 min, 1 h and 4 h for blood and 1 h, 4 h and 24 h for urine collection.

2.14. Ex vivo analysis

Mice were injected intravenously with rhodamine-labeled lectin (Vector Laboratories, Ltd., UK), for staining of blood vessels, 15 min before sacrifice and 48 h after sample injection. Tumors, liver, spleen, heart, lungs, uterus, intestines, muscle and skin were collected, weighted and analyzed by 2D Fluorescence reflectance imaging (FRI) at the FMT at the 750 nm channel. Tumors were preserved in Tissue-Tek® O.C.T™ compound (Sakura, The Netherlands) at -80 °C for immunohistochemistry.

2.15. Histological analysis

Histological staining was performed to analyze the Cy7-labeled polyplex accumulation in tumors. Simultaneously, EGFP expression in the tissue was evaluated in order to determine the degree of transfection for both decationized pHP-PEG and cationic pHDP-PEG polyplexes. Frozen 8 μm sections were prepared, where blood vessels were previously stained by rhodamine-lectin perfusion. Sections were mounted using Mowiol and fluorescence microscopy imaging was performed using an Axio Imager M2 microscope and a high-resolution AxioCam MRm Rev.3 camera, at magnification 40 \times . Images of 3 independent sections per animal were further post-processed using AxioVision Rel 4.8 software (Carl Zeiss Microimaging GmbH, Göttingen, Germany) and analyzed for Cy7 signal (polyplex accumulation) and EGFP signal (transfection efficiency).

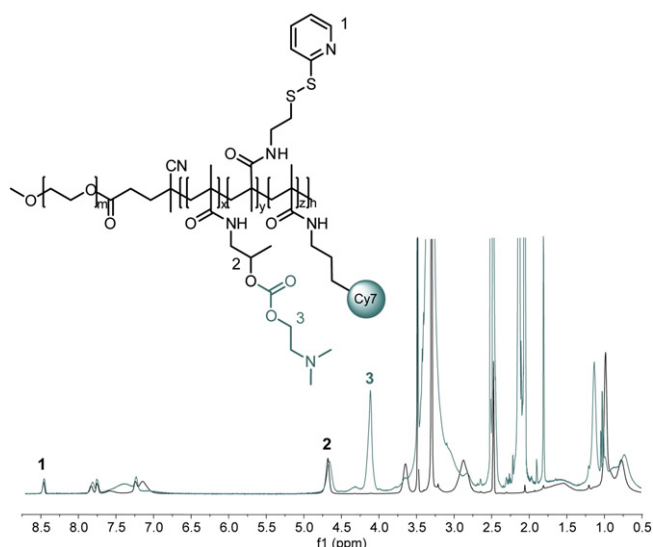


Fig. 1. ^1H NMR spectra of p(HPMA-co-PDTEMA-co-APMA) and p(HPMA-DMAE-co-PDTEMA-co-Cy7)-b-PEG in DMSO.

2.16. Statistical analysis

Statistical analysis for comparison between means was performed with the software GraphPad Prism 5 (GraphPad Software Inc., La Jolla, California, USA) and a two-tailed paired Student's *t*-test was used, where $p < 0.05$ was considered to represent statistical significance.

3. Results and discussion

3.1. Synthesis of fluorescently labeled p(HPMA-DMAE-co-PDTEMA)-b-PEG

The stability evaluation by fSPT and the *in vivo* evaluation by 3D-FMT of decationized polyplexes required the synthesis of Cy5- and Cy7-labeled pHDP-PEG, which was performed in 3 steps (Scheme 1). First, p(HPMA-co-PDTEMA-co-APMA)-b-PEG was synthesized via free-radical polymerization of HPMA, PDTEMA and APMA using mPEG₂-ABCPA as a PEG₅₀₀₀ bi-functionalized azo macronitiator [40] (Scheme 1). The yield of polymerization was close to 75%. The results of the analysis of the polymer by ^1H NMR (Fig. 1), GPC and TNBSA assay are given in Table 1. The different monomers were incorporated in the polymer close to the feed ratio. The M_n calculated by ^1H NMR (44.0 kDa) is in good agreement with GPC (34.4 kDa, PDI = 1.6). The incorporation of PDTEMA was confirmed by UV, and a value of 821 ± 43 nmol per mg of polymer was found, which is very close to the value calculated by GPC (863 nmol per mg of polymer; thus around 40 units of PDTEMA were present per polymer chain). The TNBSA assay showed that approximately 2 units APMA per polymer chain were present.

NHS-functionalized dyes were conjugated to p(HPMA-co-PDTEMA-co-APMA)-b-PEG by reaction with the primary amines of APMA for 36 h using a 2 molar excess of reactive dyes (Scheme 2). After reaction, the crude product was analyzed with GPC, and the coupling efficiency was determined by GPC analysis of the AUC of the polymer and unreacted dye peaks (detection at 646 nm (Cy5 coupling) or 700 nm

(Cy7 coupling)). The obtained chromatograms revealed that the AUC for each peak was close to 50% for both reactions, demonstrating that the amine groups of the polymers were quantitatively modified with dye molecules. Fig. 2a shows the GPC chromatogram of the crude product from Cy7 coupling reaction. In the third step, the crude product (e.g. p(HPMA-co-PDTEMA-co-(Cy5/Cy7)-b-PEG) was reacted with DMAE-Cl (Scheme 2) to yield the cationic polymer p(HPMA-DMAE-co-PDTEMA-co-(Cy5/Cy7)-b-PEG. After purification of the polymer by extensive dialysis, ^1H NMR (Fig. 1) showed that the integral ratio between peaks at $\delta 4.2$ ppm (bs, OCH_2CH_2), HPMA-DMAE) and $\delta 4.6$ ppm (bs, $\text{CH}_2\text{CHCH}_3\text{O}$, HPMA-DMAE) was close to 2, confirming a quantitative reaction of the OH groups of HPMA with DMAE-Cl. GPC analysis of the final purified products showed complete removal of the unreacted dyes for both Cy5- and Cy7-labeled polymer (e.g. Fig. 2b for Cy7-labeled polymer). The modification of HPMA groups with the cationic DMAE groups after dye coupling was chosen over the direct polymerization of HPMA-DMAE monomer [33,34] because of the incompatibility of the carbonate ester bond in HPMA-DMAE with primary amines.

3.2. Preparation of fluorescently labeled decationized pHP-PEG polyplexes

Polyplexes of pHDP-PEG were formed through the 3-step process [33,34] (Scheme 3). The preparation of Cy5 or Cy 7-labeled decationized polyplexes started with the complexation of the cationic block copolymer p(HPMA-DMAE-co-PDTEMA-co-Cy5/Cy7)-b-PEG (pHDP-PEG) with pDNA via electrostatic interactions. The interchain disulfide crosslinking of the polyplexes was performed via thiol-disulfide exchange reaction by the addition of DTT corresponding to a 50% molar equivalent of the PDS groups of the polymer, to induce self-crosslinking of the polyplexes [45], yielding cationic pHDP-PEG polyplexes. To obtain decationized polyplexes from cationic precursors, decationization was performed by the removal of the DMAE cationic side groups linked via carbonate ester bond to the HPMA backbone at pH 8.5 for 6.5 h. This process yields p(HPMA-co-PDTEMA-co-Cy5/Cy7)-b-PEG (pHP-PEG) decationized polyplexes. The structural stabilization and pDNA entrapment was solely dependent on the interchain disulfide crosslinks in the pHDP-PEG core.

An overview of the biophysical properties of both the decationized pHDP-PEG and cationic pHDP-PEG polyplexes by DLS and zeta potential measurements is shown in Table 2. Polyplexes were prepared by complexing the polymer with pDNA at an optimal N/P = 4 regarding their biophysical and *in vitro* transfection properties [33]. Firstly, pHDP-PEG formed nanosized particles with a diameter of 140 ± 5 nm and a positive zeta potential of $+11 \pm 3$. After decationization, pHP-PEG polyplexes had a size of 142 ± 8 nm and a slightly negative zeta potential of -4 ± 2 mV. The decrease in zeta potential, from cationic to decationized arises from the loss of the cationic DMAE groups from the pHDP and from the entrapped pDNA in the core [33]. The loss of electrostatic interactions between the polymer and pDNA potentially leads to some hydration and thus slight swelling of the polyplex core, however by using a zero-length crosslinking agent such as DTT, this effect is limited. Size is a particularly critical property for the biodistribution of nanoparticles [47], however, here this variable is ruled out by evaluation polyplexes of very similar size.

Both decationized pHDP-PEG and cationic pHDP-PEG polyplexes were complementarily analyzed by NTA, a technique that allows the simultaneous analysis of individual particles in a suspension and gives

Table 1
p(HPMA-co-PDTEMA-co-APMA)-b-PEG characteristics as determined by GPC, ^1H NMR, UV spectroscopy and TNBSA assay.

GPC		NMR		NMR, TNBSA	UV
M_n (kDa)	PDI	M_n (kDa)	Feed	Polymer	nmol _{PDS} /mg _{polymer}
34.4	1.6	44.0	HPMA-DMAE/PDTEMA/APMA 1/0.20/0.01	HPMA-DMAE/PDTEMA/APMA 1/0.19/0.01	821.0 ± 43.3

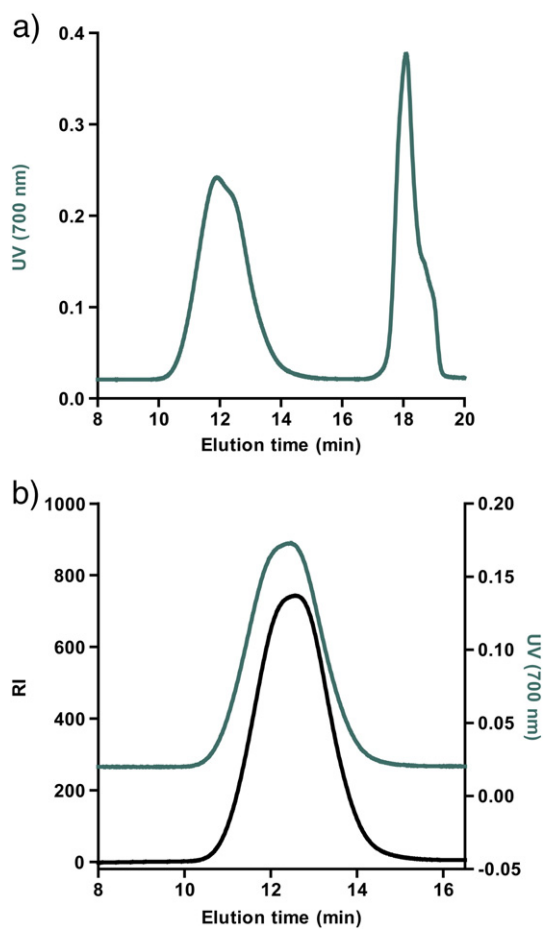


Fig. 2. GPC chromatograms (a) UV detection at 700 nm of the crude product from coupling of Cy7-NHS to p(HPMA-co-PDTEMA-co-APMA)-b-PEG, using a 2 molar equivalent excess of Cy7-NHS to primary amines in the polymer. (b) Refractive index signal (RI) and UV signal at 700 nm of the final purified p(HPMA-co-PDTEMA-co-Cy7)-b-PEG polymer.

information of the true size distribution (Fig. 3) [48]. Similarly to the DLS results, decationized polyplexes and cationic polyplexes showed comparable average sizes (around 145–150 nm). Importantly, the size distribution measured by NTA displayed similar distribution profiles: for both particles, when prepared at high concentration for *in vivo* applications (400 µg/mL), around 90% of the polyplexes had a size below 210 nm. Size and charge measurements demonstrate that introduction of cyanine fluorophores and preparation of polyplexes at high concentration did not affect significantly the polyplexes properties [33,34].

3.3. Stability of decationized pHP-PEG polyplexes in human plasma

The stability of cationic pHDP-PEG and decationized pHP-PEG Cy5-labeled was evaluated by incubation at 37 °C in human plasma. The size distribution of the polyplexes in plasma was determined by fSPT

Table 2

Particle z-average diameter (Z-avg) and polydispersity index (PDI) determined by DLS, and particle charge (ζ Pot) determined by zeta potential measurements, of decationized pHP-PEG and cationic pHDP-PEG polyplexes. Results are expressed as mean \pm SD (n = 3).

Polyplexes	DLS		Zetasizer
	Z-ave (nm)	PDI	ζ Pot (mV)
pHP-PEG	142 \pm 8	0.20 \pm 0.01	-4 \pm 2
pHDP-PEG	140 \pm 5	0.19 \pm 0.01	11 \pm 3

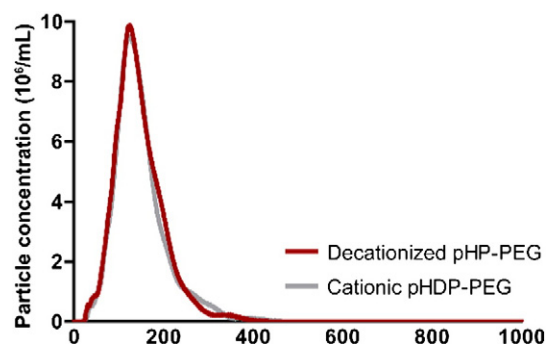


Fig. 3. Decationized pHP-PEG and cationic pHDP-PEG polyplexes size distribution determined by NTA in PBS at 25 °C.

and compared to the distributions obtained when polyplexes were diluted in HEPES buffer pH 7.4 (Fig. 4). The method is based on single particle tracking analysis of fluorescent particles which allows the determination of precise size distributions in media with intrinsic light scattering such as undiluted biological fluids [36]. The fSPT technique is especially important to gain information on the possible aggregation of nanoparticles. When Cy5-labeled polyplexes, both cationic and decationized, were measured in HEPES buffer by fSPT, comparable size distributions to the ones obtained by DLS and NTA were observed. The distribution was relatively narrow, with a peak around 200 nm. When the cationic pHDP-PEG polyplexes were incubated in human plasma for 1 h, a clear change in the distribution profile was observed and a higher average size (\sim 300 nm) as well as polyplexes with >400 nm in diameter were clearly detected. Upon incubation for 48 h, the average size (560 nm) and the population of polyplexes with diameter >400 nm were increased. The instability detected for crosslinked cationic

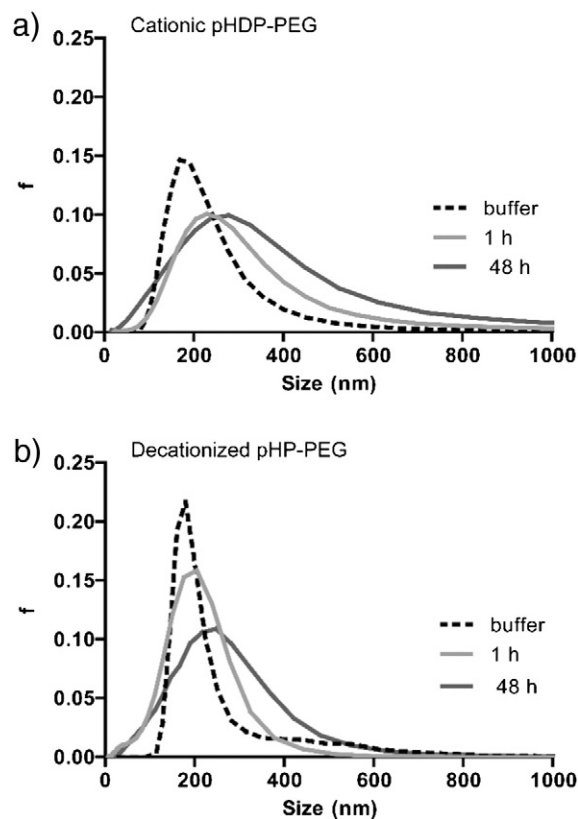


Fig. 4. The size distribution of cationic pHDP-PEG and decationized pHP-PEG polyplexes as determined by fSPT after incubation in 90% (v/v) human plasma at 37 °C for 1 h and 48 h. Size distribution was also determined in 20 mM HEPES pH 7.4.

polyplexes likely occurs due to insufficient shielding of the positive charge of the polyplexes by PEG and consequent interaction of polyplexes with negatively charged proteins from plasma. Indeed, Table 2 shows that the cationic pHDP-PEG polyplexes have a positive zeta-potential. Importantly, when pHDP-PEG decationized polyplexes were incubated with human plasma for 1 h, only a slight change of the size distribution was observed, and the peak of the distribution remained unchanged. Consequently, crosslinked decationized polyplexes retained their integrity in biological fluids, and did not show aggregation (mediated e.g. by plasma proteins). For example, almost no polyplexes with a diameter of >400 nm were detected which is in great contrast with the cationic polyplexes. In line with this, also after incubation the polyplexes for 48 h the size distribution only changed slightly, without any aggregation detected. A slight increase in size after 48 h probably occurs due to protein adsorption to the polyplexes as a consequence of loss of PEG density due to continuous hydrolysis of the ester bond linking PEG chains with HPMA-co-PDTEMA block. PEG is essential to stabilize nanoparticles, avoid aggregation and protein adsorption in blood. This is quite evident for cationic particles [12,15,16], but essential for anionic particles as well [49,50].

The stability assessment is especially important for systemic administration of polyplexes. Firstly in terms of safety, cationic polymer-based systems, when administered intravenously lead to the formation of aggregates by interactions with negatively charged blood components. These aggregates can be retained in the lungs causing embolism and consequent death [12]. Other severe consequences comprise liver necrosis and as uncontrollable distribution and expression [10]. The assessment of the stability is also important to ensure the success of these systems when applied intravenously. In order to target tumors, polyplexes should also possess prolonged circulation and maintain a stable size in the order of few hundreds of nanometers to reach and extravasate in the tissue leaky tumor vasculature, via EPR effect [51–53]. Decationization of polyplexes complemented by the shielding properties of PEG, significantly improves the stability of polyplexes when compared to their cationic polyplexes and therefore increasing the chances to target tumors via EPR.

3.4. *In vitro* and *in vivo* toxicity assessment

To assess the toxicity of the decationized pHDP-PEG and cationic pHDP-PEG, the polymers were evaluated *in vitro* with HUVEC cells via MTT assay in an acute (24 h) and a long term toxicity test (Fig. 5a) and *in vivo* with a zebrafish embryo model (Fig. 5b and c) with different polymer concentrations (0.1 to 3 mg/mL). The cationic polymer b-PEI, a commonly used transfection agent, was used as a positive control for toxicity [37].

The *in vitro* toxicity was tested in HUVEC cells due their high sensitivity toward transfection agents [54]. The MTT test revealed that decationized pHDP-PEG had no effect on the cell viability, in any of the concentrations tested, when incubated with the cells for 24 h. Only a slight decrease on the cell viability was found in case incubation was prolonged for 72 h. The *in vitro* evaluation of the cationic pHDP-PEG polymer showed that the polymer lead to decrease in cell viability with increasing concentrations, to a level of 70% cell viability for 3 mg/mL when tested for acute toxicity. For long term toxicity test (72 h incubation) the cytotoxic effects were even more pronounced and at 1 mg/mL already lead to decrease in cell viability to 20%. In the case of b-PEI extreme toxicity was observed, at the lowest concentration tested (0.1 mg/mL) b-PEI induced complete cell death in both acute and long terms *in vitro* toxicity test.

The zebrafish eggs were incubated with increasing polymer concentrations, and teratogenic effect and the mortality potential on the different zebrafish embryonic stages were monitored microscopically for a period of 72 h. The neutral polymer pHDP-PEG showed no effect on the fish viability for any of the concentrations tested. Developmental defects and delayed hatching were observed only for the highest concentration

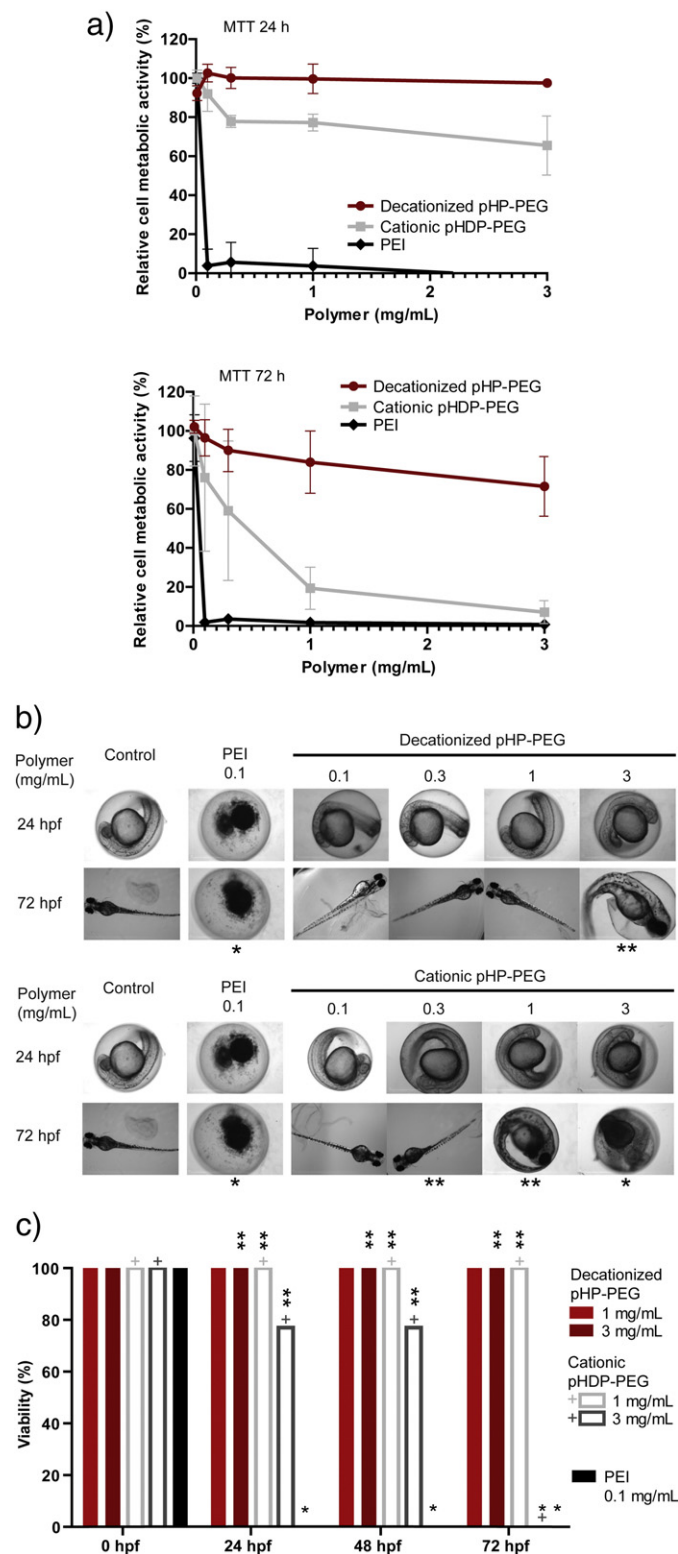


Fig. 5. Safety evaluation of decationized polyplexes (a) HUVEC cell relative viability relative upon exposure for 24 h or 72 h to decationized pHDP-PEG, cationic pHDP-PEG and b-PEI from 0.1 mg/mL to 3 mg/mL. Results are expressed as mean \pm SD (n = 4). (b) Representative images of zebrafish embryo development upon exposure to decationized pHDP-PEG and to cationic pHDP-PEG at concentrations ranging from 0.1–3 mg/mL. *significant mortality, **significant developmental defects (i.e. decreased pigmentation, delayed hatching ratio and slower heartbeat). (c) zebrafish survival upon exposure to decationized pHDP-PEG and cationic pHDP-PEG polymers in comparison with b-PEI (*100% mortality; n = 6). hpf (hours post-fertilization).

tested (3 mg/mL). For the cationic polymer pHDP-PEG a significant decrease on zebrafish viability was observed at 3 mg/mL, resulting in 100% fish death at 72 h. Mortality was also detected at a very early stage of the development (1 out of 6) together with a slower heartbeat in the surviving ones. Furthermore, the cationic pHDP-PEG also interfered significantly in the embryonic development of the fishes. A decrease in the pigmentation was observed from a concentration of 0.3 mg/mL onwards, no hatching was observed at 48 h for 1 mg/mL and at 3 mg/mL all fish had a decreased heartbeat. In line with the *in vitro* test, b-PEI was again responsible for extreme toxicity, by inducing complete fish death at 0.1 mg/mL even at early stages of development.

Evident toxicity was induced by the biodegradable cationic pHDP-PEG polymer, particularly observed on long term (observed in HUVEC cells and zebrafish). Toxicity is obviously less than b-PEI, but by using a wide range of concentrations and exposure times we evidence that biodegradability is not sufficient for a completely safe gene delivery system. We demonstrate not only effects on cell and organism viability but also on the teratogenicity potential observed in zebrafish embryos at lower concentrations. In great contrast, a practically innocuous profile of the decationized pHDP-PEG was observed in short and long terms *in vitro* and in the zebrafish assay. This contrast between decationized and cationic polymers proves the importance of developing gene delivery systems based on neutral polymers in order to build safe vectors.

3.5. *In vivo* biodistribution and tumor accumulation

Cy7-labeled pHDP-PEG decationized and pHDP-PEG cationic polyplexes were intravenously injected into mice bearing subcutaneous A431 tumors, and their biodistribution and tumor accumulation were non-invasively monitored using 3D μ CT-FMT. Hybrid μ CT-FMT method allows the effective *in vivo* visualization of near-infrared (NIR) dye labeled nanomedicines, and the (semi-) quantification of their accumulation in tumors and healthy organs. By fusing and reconstructing 3D FMT data with μ CT images, and by performing absorption pre-scans, a more accurate assignment of fluorescence signals to deep internal organs tissues can be performed [38,55,56]. Compared to the 2D FRI, 3D μ CT-FMT is not limited to superficial visualization, animal sacrificing is not required.

In parallel with 3D μ CT-FMT images, blood circulation kinetics was determined by 2D FRI signals of blood and urine collected at different time points p.i. (Fig. 6). Quantification of polyplex signals in blood showed that there was a very rapid decrease of the %ID for both cationic and decationized polyplexes which typical for polyplex systems when administered intravenously [15,16,22,57,58] (Fig. 6a). Importantly, a significant higher blood circulation time was observed for decationized pHDP-PEG polyplexes. Decationized polyplexes showed a higher signal in blood at all time points when compared to cationic pHDP-PEG. The elimination rate via kidneys was determined by detecting 2D FRI signals from urine (Fig. 6b). High Cy7 %ID was detected in urine 15 min p.i. for both groups, followed by a rapid decrease 4 h p.i. Most likely, this was due to a rapid glomerular filtration of low M_w polymer fraction that is not built in the polyplexes. This fraction of polymers is the same for both cationic and decationized polyplexes, as confirmed by the similar signals found for both polyplexes.

As shown in Fig. 7, using μ CT imaging, tumors, liver, heart, lungs, kidneys and bladder were manually segmented, to assign the NIR fluorescence signals from the polyplexes at different times points, as previously described [38]. Next, the accumulation of pHDP-PEG decationized and pHDP-PEG cationic polyplexes in tumors and different organs was quantified. Quantification in tumors showed higher normalized %ID detected in tumors for decationized polyplexes when compared to their cationic counterpart 48 p.i. Also, for decationized polyplexes increasing accumulation in tumors was observed with the highest accumulation point at 48 h p.i. In contrast, for cationic polyplexes an accumulation plateau was rapidly reached (within 15 min), which have been previously observed for other cationic systems [22].

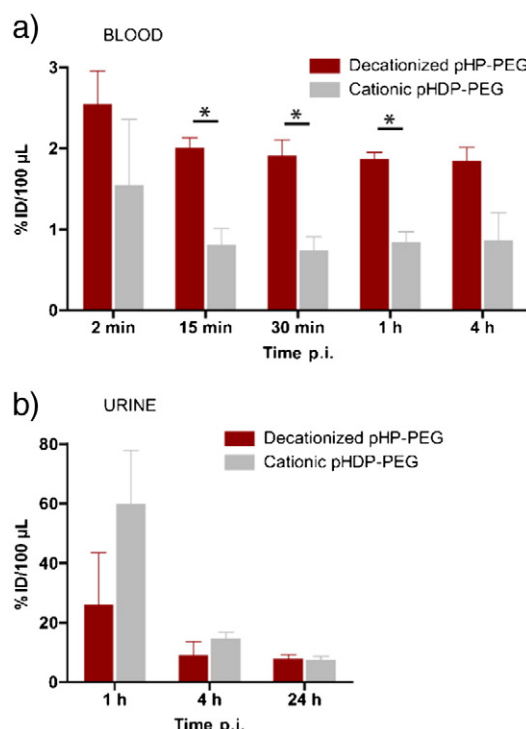


Fig. 6. 2D FRI quantification as %ID (per 100 μ L) of decationized pHDP-PEG and cationic pHDP-PEG Cy7-labeled polyplexes signals in (a) blood and (b) urine at different time points p.i. Results are expressed as mean \pm SD ($n = 3$). * $p < 0.01$ (t-test).

Both polyplexes showed a high accumulation in healthy organs, mainly in liver and kidneys 15 min p.i. However, in the case of decationized polyplexes there was a rapid signal decrease at 4 h p.i. resulting in an apparent lower accumulation of decationized polyplexes in liver and kidneys, when compared to cationic polyplexes. Most likely decationized polyplexes were able to maintain a population of polyplexes in the circulation or rapidly accumulated in the different organs, but due to their improved ability to maintain small and stable size in biological fluids (Fig. 4) together with their low unspecific uptake properties [33,34], polyplexes can reenter the blood circulation and accumulate in tumor tissues. This behavior has been previously described for other nanoparticulate systems [59,60].

The major organ of polyplex accumulation of polyplexes was the liver, which contains Kupffer cells as part of the mononuclear phagocyte system (MPS) which are responsible for phagocytic activity and rapid clearance of nanoparticles *in vivo* [60–62]. Liver accumulation is very critical for PEGylated polymer-DNA complexes [15,22,57]. The ability of decationized polyplexes to escape from liver and remain stable in circulation more efficiently determines their higher circulation *in vivo*. As hypothesized, PEG is not able to completely shield cationic particles, leading to unspecific uptake or opsonization, which in turn leads to decreased circulation time when compared to the decationized polyplexes.

Significant NIR signal was noticed in the bladder 15 min p.i. for both groups with similar degrees and with a rapid drop of signal 4 h p.i. The signal profiles are in line with the results determined by 2D FRI in urine and as quantified, the initial elimination into the bladder corresponds to 15–20 total %ID.

Accumulation in kidneys was also pronounced, with a tendency of higher accumulation of cationic polyplexes. Kidney accumulation has been previously found for polymeric vectors [57,63,64]. Kidney retention can be particularly critical for polycation-based systems. The nanoparticles within the kidney will have to pass through the glomerulus which is in close contact with glomerular basement membrane (GBM), a 300- to 350-nm-thick basal lamina rich in negatively charged

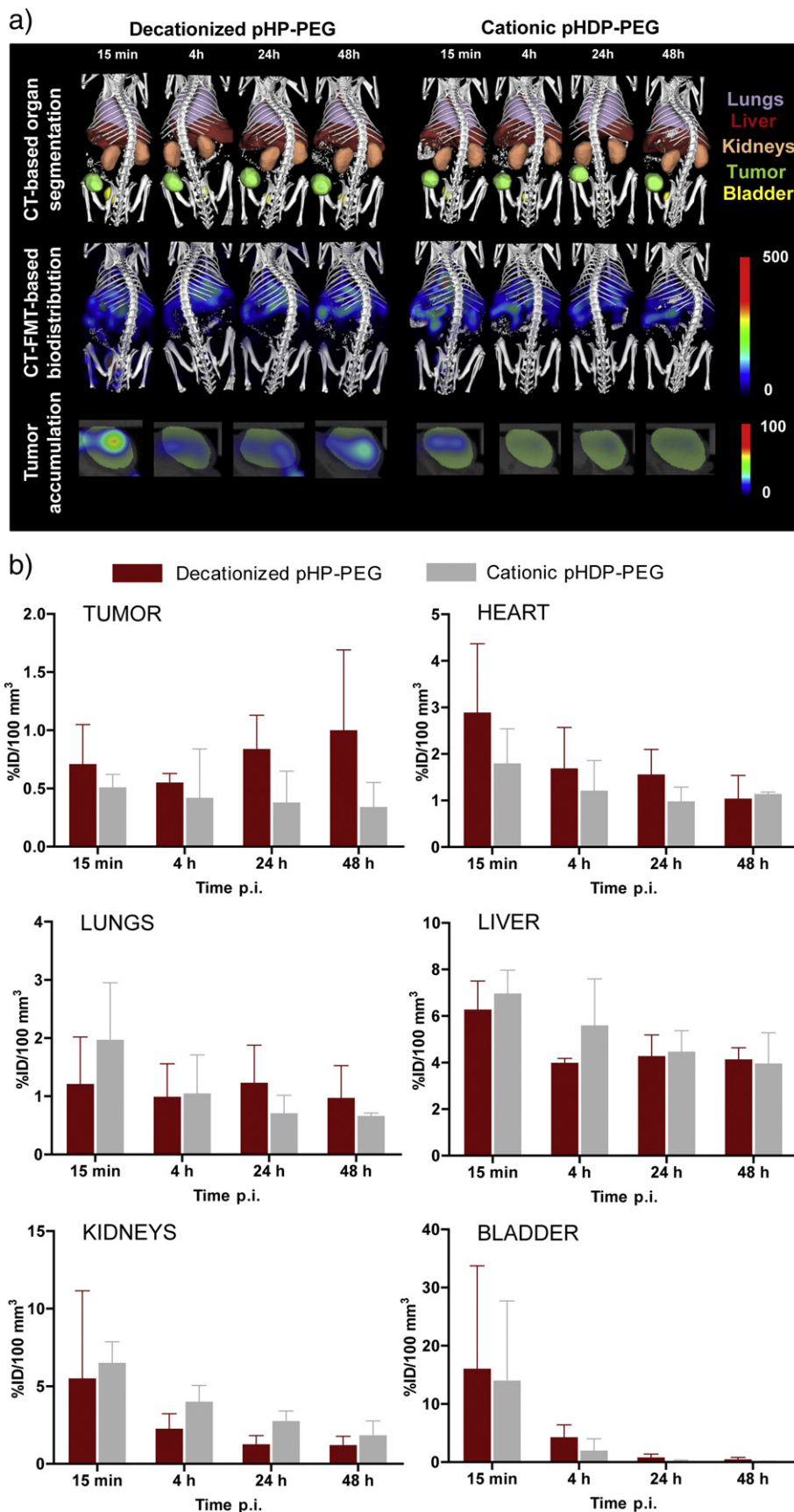


Fig. 7. Noninvasive *in vivo* 3D CT-FMT imaging of the biodistribution and tumor accumulation of decationized pHHP-PEG and cationic pHDP-PEG Cy7-labeled polyplexes. (a) Principle of 3D CT-FMT imaging: anatomical information obtained using μ CT is used to assign the Cy7 signals coming from polyplexes to a specific organ or tissue of interest. The images were obtained at 15 min, 4 h, 24 h and 48 h p.i. and show Cy7 localization mainly in liver (red) and kidney (orange). Tumor accumulation was more prominent for decationized polyplexes. (b) Quantification of the tumor accumulation and biodistribution of Cy7-labeled decationized pHHP-PEG and cationic pHDP-PEG polyplexes in tumors, liver, lungs, kidney, bladder and heart, expressed as %ID per 100 mm³ tissue. Results are presented as mean \pm SD ($n = 3$).

proteoglycans, to which particles of around 100 nm can access [65]. Ultimately, particle retention in the GBM is driven by the surface charge, leading to cationic particles to be retained [66].

It is also important to point out that no significant lung deposition was observed for both systems. Lung capillaries are among the smallest blood vessels and sieving might occur in case aggregates are formed [60], which is normally associated with acute toxicity or off-targeting transfection [10,12]. Our results demonstrate that both polyplexes do not induce acute aggregation *in vivo* in line with the results shown in Fig. 4.

3.6. *Ex vivo* for probe accumulation and *in vivo* transfection

After the 3D μ CT-FMT procedure at 48 p.i., mice were sacrificed and tumors, lungs, spleen, kidneys, heart skin, intestines and muscle were analyzed using 2D FRI (Fig. 8a and b). The NIR signals from tumors and several physiologically relevant healthy organs (liver, spleen, lungs and kidneys) were quantified and compared for both Cy7-labeled decationized pHDP-PEG and cationic pHDP-PEG polyplexes. 2D FRI quantification determined *ex vivo* supports and further validates the results of the 3D μ CT-FMT analysis. In the case of 2D FRI measurements, a significantly higher accumulation in the tumors was observed for decationized polyplexes. As determined by 3D μ CT-FMT, 3 times higher accumulation for decationized polyplexes was also found. The tendency of a lower accumulation in healthy organs was also observed for decationized polyplexes with 2D FRI. Similar accumulation in liver was observed for both polyplexes 48 p.i., but in the case of spleen and kidneys higher accumulation was observed for cationic polyplexes. The spleen, together with liver constitutes the MPS. In the spleen nanoparticles are sieved and subsequently taken up by macrophages or splenocytes [60,61]. The apparent lower retention of decationized polyplexes in the spleen further demonstrates the advantages of decationized polyplexes.

Cryosections of tumors collected 48 p.i. were analyzed using fluorescence microscopy, to validate the *in vivo* and *ex vivo* Cy7-labeled polyplex accumulation results (Fig. 8c and d). By quantifying the Cy7 signals on tumor sections of both groups, 2 times higher signal was observed for decationized polyplexes with statistical significance. Microscopy was also used to determine the *in vivo* tumor transfection potential of both decationized pHDP-PEG and cationic pHDP-PEG polyplexes containing EGFP encoding pDNA (Fig. 8c and d). The EGFP signal, which allows to infer on the transfection ability of polyplexes, was similar for both systems, even though significant differences were found in NIR tumor accumulation. Transfection requires polyplexes' (extensive) uptake by the target cells. The lower transfection ability of decationized polyplexes is therefore likely attributed to its low degree of unspecific uptake. We also showed that uptake can be triggered by the introduction of a targeting ligand at the surface of decationized polyplexes [33,34]. Furthermore, the introduction of targeting ligands is important to accelerate the rate of cellular uptake of polyplexes and prevent premature reduction of disulfide crosslinks before cell entry due to the presence of secreted and cell membrane thiols [67]. Cationic polyplexes, in contrast, are known to be taken up extensively by electrostatic interaction with cell membrane anionic components [3,68,69]. The transfection ability of cationic pHDP-PEG polyplexes is in line with previous findings of pHPPA-DMAE to induce *in vivo* transfection in tumors [70].

It should be noticed that the ability of cationic polyplexes to transfect cells more efficiently has counterproductive effects because it also leads to an increased probability of off-targeting expression, especially when high accumulation is observed in liver, spleen and kidneys. Unwanted

transfection in healthy organs has been previously observed particularly in liver and lungs [16,22,71]. In the recent years, several strategies have been developed to introduce target transfection with encouraging results [58,63,64,72]. Decationized polyplexes can potentiate further specific transfection in tumors especially when a targeting ligand is introduced [34]. Furthermore, due to its low toxic and low teratogenic potential, decationized polyplexes are less limited to dose and repeated administration restrictions, resulting in a promising and attractive system for further optimization strategies and testing.

Future studies have to be focused on deeper evaluation of transfection ability of optimized formulations of decationized polyplexes. Optimization for a better *in vivo* performance can be done by using targeted systems or by optimizing the polymer structure, for example by determining the best PEG block molecular weight and density [73,74] or by introduction of hydrophobic groups in the core of polyplexes groups into polyplexes [75]. In a next step, therapeutic genes should be used to determine the therapeutic potential of decationized polyplexes.

4. Conclusions

Decationized polyplexes, unlike conventional polycationic polymeric gene delivery systems, are based on neutral polymers. In the present study, we demonstrate that the neutral polymer pHDP-PEG when tested for toxicity *in vitro* with HUVEC cells showed a very good cytocompatibility in both acute and long term toxicity test. Furthermore, an *in vivo* zebrafish toxicity assay revealed that pHDP-PEG did not induce fish mortality and, importantly, showed a much lower teratogenicity potential when compared with its cationic counterpart. This apparent safe polymer formed polyplexes with a high stability in biological fluids, as determined by fSPT, which validated its applicability *in vivo* applicability for systemic administration. Using noninvasive optical imaging (3D μ CT-FMT) and complementary *ex vivo* analysis we demonstrated that by removing the cationic groups of polyplexes, we obtained a system with higher tumor accumulation, most likely due to their longer blood circulation and apparent decreased accumulation in healthy organs. *Ex vivo* analysis validated the optical imaging results and histology in tumor cryosections and showed that decationized polyplexes induced transgene expression *in vivo*.

The described strategy for preparing decationized polyplexes and the results reported are an important contribution to take into consideration to develop safer and more efficient nonviral gene delivery systems.

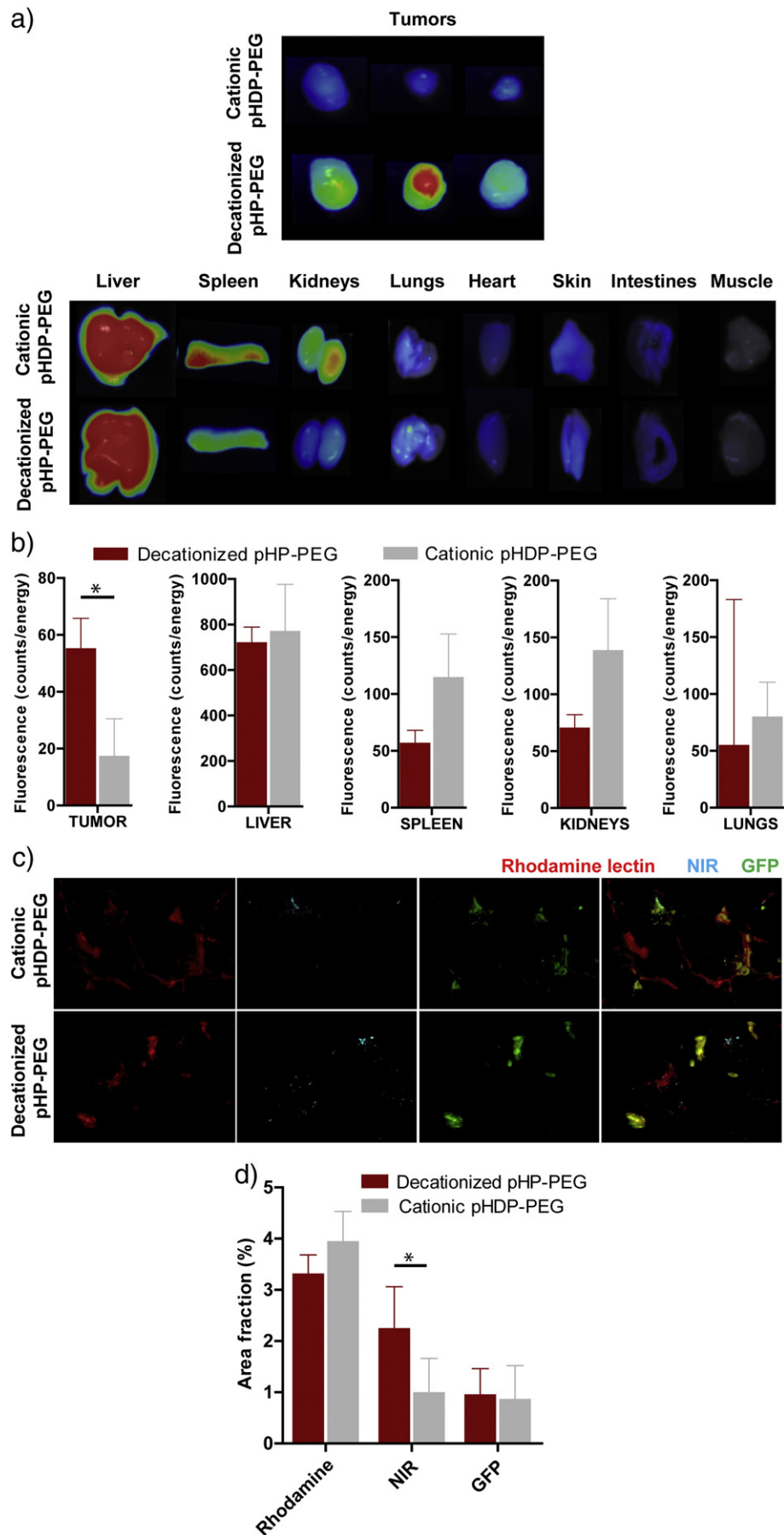
Acknowledgment

The authors gratefully acknowledge financial support by the Portuguese Foundation for Science and Technology (FCT) (grant SFRH/BD/47085/2008), by the German Academic Exchange Service (DAAD; 290084/2011-3), by the DFG (LA 2937/1-2), by the European Union (COST – Action TD1004), and by the European Research Council (ERC Starting Grant 309495: NeoNaNo).

References

- [1] L.W. Seymour, A.J. Thrasher, Gene therapy matures in the clinic, *Nat. Biotechnol.* 30 (2012) 588–593.
- [2] T. Wirth, N. Parker, S. Ylä-Herttuala, History of gene therapy, *Gene* 525 (2013) 162–169.
- [3] M.A. Mintzer, E.E. Simanek, Nonviral vectors for gene delivery, *Chem. Rev.* 109 (2008) 259–302.
- [4] W. Li, F.C. Szoka Jr., Lipid-based nanoparticles for nucleic acid delivery, *Pharm. Res.* 24 (2007) 438–449.

Fig. 8 *Ex vivo* analysis. (a) Representative *ex vivo* 2D FRI assessment of the tumor accumulation and biodistribution of decationized pHDP-PEG and cationic pHDP-PEG Cy7-labeled polyplexes at 48 h p.i. (b) Quantification of polyplex accumulation in tumors and healthy organs. Results are expressed as mean \pm SD ($n = 3$). (c–d) Fluorescence microscopy imaging (c) and quantification (d) of decationized pHDP-PEG and cationic pHDP-PEG Cy7-labeled polyplexes (blue) accumulating in tumors at 48 h p.i. and inducing EGFP expression (green). Blood vessels are labeled using rhodamine-lectin (red). Results are expressed as mean \pm SD ($n = 3$). * $p < 0.05$ (t-test).



- [5] J. Luten, C.F. van Nostrum, S.C. De Smedt, W.E. Hennink, Biodegradable polymers as non-viral carriers for plasmid DNA delivery, *J. Control. Release* 126 (2008) 97–110.
- [6] S.Y. Wong, J.M. Pelet, D. Putnam, Polymer systems for gene delivery – past, present, and future, *Prog. Polym. Sci.* 32 (2007) 799–837.
- [7] E. Mastrobattista, M.A.E.M. van der Aa, W.E. Hennink, D.J.A. Crommelin, Artificial viruses: a nanotechnological approach to gene delivery, *Nat. Rev. Drug Discov.* 5 (2006) 115–121.
- [8] A. Yousefi, G. Storm, R. Schiffelers, E. Mastrobattista, Trends in polymeric delivery of nucleic acids to tumors, *J. Control. Release* 170 (2013) 209–218.
- [9] P. Midoux, C. Pichon, J.-J. Yaouanc, P.-A. Jaffrès, Chemical vectors for gene delivery: a current review on polymers, peptides and lipids containing histidine or imidazole as nucleic acids carriers, *Br. J. Pharmacol.* 157 (2009) 166–178.
- [10] P. Chollet, M.C. Favrot, A. Hurbini, J.-L. Coll, Side-effects of a systemic injection of linear polyethylenimine–DNA complexes, *J. Gene Med.* 4 (2002) 84–91.
- [11] C.M. Ward, M.L. Read, L.W. Seymour, Systemic circulation of poly(L-lysine)/DNA vectors is influenced by polycation molecular weight and type of DNA: differential circulation in mice and rats and the implications for human gene therapy, *Blood* 97 (2001) 2221–2229.
- [12] M. Ogris, S. Brunner, S. Schuller, R. Kircheis, E. Wagner, PEGylated DNA/transferrin-PEI complexes: reduced interaction with blood components, extended circulation in blood and potential for systemic gene delivery, *Gene Ther.* 6 (1999) 595–605.
- [13] R. Duncan, The dawning era of polymer therapeutics, *Nat. Rev. Drug Discov.* 2 (2003) 347–360.
- [14] C.F. Jones, R.A. Campbell, A.E. Brooks, S. Assemi, S. Tadjiki, G. Thiagarajan, C. Mulcock, A. S. Weyrich, B.D. Brooks, H. Ghandehari, D.W. Grainger, Cationic PAMAM dendrimers aggressively initiate blood clot formation, *ACS Nano* 6 (2012) 9900–9910.
- [15] F.J. Verbaan, C. Oussoren, C.J. Snel, D.J.A. Crommelin, W.E. Hennink, G. Storm, Steric stabilization of poly(2-(dimethylamino)ethyl methacrylate)-based polyplexes mediates prolonged circulation and tumor targeting in mice, *J. Gene Med.* 6 (2004) 64–75.
- [16] M. Harada-Shiba, K. Yamauchi, A. Harada, I. Takamisawa, K. Shimokado, K. Kataoka, Polyion complex micelles as vectors in gene therapy – pharmacokinetics and *in vivo* gene transfer, *Gene Ther.* 9 (2002) 407–414.
- [17] M.H. Lee, Z. Yang, C.W. Lim, Y.H. Lee, S. Dongbang, C. Kang, J.S. Kim, Disulfide-cleavage-triggered chemosensors and their biological applications, *Chem. Rev.* 113 (2013) 5071–5109.
- [18] F. Meng, W.E. Hennink, Z. Zhong, Reduction-sensitive polymers and bioconjugates for biomedical applications, *Biomaterials* 30 (2009) 2180–2198.
- [19] D.S. Manickam, J. Li, D.A. Putt, Q.-H. Zhou, C. Wu, L.H. Lash, D. Oupický, Effect of innate glutathione levels on activity of redox-responsive gene delivery vectors, *J. Control. Release* 141 (2010) 77–84.
- [20] D. Oupický, R.C. Carlisle, L.W. Seymour, Triggered intracellular activation of disulfide crosslinked polyelectrolyte gene delivery complexes with extended systemic circulation *in vivo*, *Gene Ther.* 8 (2001) 713–724.
- [21] Y. Vachutinsky, M. Oba, K. Miyata, S. Hiki, M.R. Kano, N. Nishiyama, H. Koyama, K. Miyazono, K. Kataoka, Antiangiogenic gene therapy of experimental pancreatic tumor by sFlt-1 plasmid DNA carried by RGD-modified crosslinked polyplex micelles, *J. Control. Release* 149 (2011) 51–57.
- [22] H.K. de Wolf, C.J. Snel, F.J. Verbaan, R.M. Schiffelers, W.E. Hennink, G. Storm, Effect of cationic carriers on the pharmacokinetics and tumor localization of nucleic acids after intravenous administration, *Int. J. Pharm.* 331 (2007) 167–175.
- [23] D. Oupický, M. Ogris, K.A. Howard, P.R. Dash, K. Ulbrich, L.W. Seymour, Importance of lateral and steric stabilization of polyelectrolyte gene delivery vectors for extended systemic circulation, *Mol. Ther.* 5 (2002) 463–472.
- [24] R.J. Fields, C.J. Cheng, E. Quijano, C. Weller, N. Kristofik, N. Duong, C. Hoimes, M.E. Egan, W.M. Saltzman, Surface modified poly(β amino ester)-containing nanoparticles for plasmid DNA delivery, *J. Control. Release* 164 (2012) 41–48.
- [25] D. Fischer, Y. Li, B. Ahlemeyer, J. Krieglstein, T. Kissel, *In vitro* cytotoxicity testing of polycations: influence of polymer structure on cell viability and hemolysis, *Biomaterials* 24 (2003) 1121–1131.
- [26] S.M. Moghimi, P. Symonds, J.C. Murray, A.C. Hunter, G. Debska, A. Szewczyk, A two-stage poly(ethyleneimine)-mediated cytotoxicity: implications for gene transfer/therapy, *Mol. Ther.* 11 (2005) 990–995.
- [27] S. Choksakulnimitr, S. Masuda, H. Tokuda, Y. Takakura, M. Hashida, *In vitro* cytotoxicity of macromolecules in different cell culture systems, *J. Control. Release* 34 (1995) 233–241.
- [28] C. Loney, M. Vandenbranden, J.-M. Ruyschaert, Cationic lipids activate intracellular signaling pathways, *Adv. Drug Deliv. Rev.* 64 (2012) 1749–1758.
- [29] W.T. Godbey, K.K. Wu, A.G. Mikos, Poly(ethyleneimine)-mediated gene delivery affects endothelial cell function and viability, *Biomaterials* 22 (2001) 471–480.
- [30] K. Masago, K. Itaka, N. Nishiyama, U.-i. Chung, K. Kataoka, Gene delivery with biocompatible cationic polymer: pharmacogenomic analysis on cell bioactivity, *Biomaterials* 28 (2007) 5169–5175.
- [31] O.M. Merkel, A. Beyerle, B.M. Beckmann, M. Zheng, R.K. Hartmann, T. Stöger, T.H. Kissel, Polymer-related off-target effects in non-viral siRNA delivery, *Biomaterials* 32 (2011) 2388–2398.
- [32] K. Regnström, E.G.E. Ragnarsson, M. Köping-Höggård, E. Torstensson, H. Nyblom, P. Artursson, PEI – a potent, but not harmless, mucosal immuno-stimulator of mixed T-helper cell response and FasL-mediated cell death in mice, *Gene Ther.* 10 (2003) 1575–1583.
- [33] L. Novo, E.V.B. van Gaal, E. Mastrobattista, C.F. van Nostrum, W.E. Hennink, Decationized crosslinked polyplexes for redox-triggered gene delivery, *J. Control. Release* 169 (2013) 246–256.
- [34] L. Novo, E. Mastrobattista, C.F. van Nostrum, W.E. Hennink, Targeted decationized polyplexes for cell specific gene delivery, *Bioconjug. Chem.* 25 (2014) 802–812.
- [35] H. Maeda, J. Wu, T. Sawa, Y. Matsumura, K. Hori, Tumor vascular permeability and the EPR effect in macromolecular therapeutics: a review, *J. Control. Release* 65 (2000) 271–284.
- [36] K. Braeckmans, K. Buyens, W. Bouquet, C. Vervaeke, P. Joye, F. De Vos, L. Plawinski, L. Dœuvre, E. Angles-Cano, N.N. Sanders, J. Demeester, S.C. De Smedt, Sizing nanomatter in biological fluids by fluorescence single particle tracking, *Nano Lett.* 10 (2010) 4435–4442.
- [37] L.Y. Rizzo, S.K. Golombek, M.E. Mertens, Y. Pan, D. Laaf, J. Broda, J. Jayapaul, D. Mockel, V. Subr, W.E. Hennink, G. Storm, U. Simon, W. Jahnen-Dechent, F. Kiessling, T. Lammers, *In vivo* nanotoxicity testing using the zebrafish embryo assay, *J. Mater. Chem. B* 1 (2013) 3918–3925.
- [38] S. Kunjachan, F. Gremse, B. Theek, P. Koczera, R. Pola, M. Pechar, T. Etrych, K. Ulbrich, G. Storm, F. Kiessling, T. Lammers, *In vivo* nanotoxicity testing using the zebrafish embryo assay, *J. Mater. Chem. B* 1 (2013) 3918–3925.
- [39] A. Funhoff, C.F. van Nostrum, A. Janssen, M. Fens, D. Crommelin, W.E. Hennink, Polymer side-chain degradation as a tool to control the destabilization of polyplexes, *Pharm. Res.* 21 (2004) 170–176.
- [40] D. Neradovic, C.F. van Nostrum, W.E. Hennink, Thermoresponsive polymeric micelles with controlled instability based on hydrolytically sensitive N-isopropylacrylamide copolymers, *Macromolecules* 34 (2001) 7589–7591.
- [41] M. Talelli, C.J.F. Rijcken, S. Oliveira, R. van der Meel, P.M.P. van Bergen en Henegouwen, T. Lammers, C.F. van Nostrum, G. Storm, W.E. Hennink, Nanobody – shell functionalized thermosensitive core-crosslinked polymeric micelles for active drug targeting, *J. Control. Release* 151 (2011) 183–192.
- [42] E.V.B. van Gaal, R. van Eijk, R.S. Oosting, R.J. Kok, W.E. Hennink, D.J.A. Crommelin, E. Mastrobattista, How to screen non-viral gene delivery systems *in vitro*? *J. Control. Release* 154 (2011) 218–232.
- [43] D.R. Grassetti, J.F. Murray, Determination of sulfhydryl groups with 2,2'- or 4,4'-dithiodipyridine, *Arch. Biochem. Biophys.* 119 (1967) 41–49.
- [44] A.W. York, F. Huang, C.L. McCormick, Rational design of targeted cancer therapeutics through the multiconjugation of folate and cleavable siRNA to RAFT-synthesized (HPMA-s-APMA) copolymers, *Biomacromolecules* 11 (2010) 505–514.
- [45] J.-H. Ryu, R.T. Chacko, S. Jiwanich, S. Bickerton, R.P. Babu, S. Thayumanavan, Self-cross-linked polymer nanogels: a versatile nanoscopic drug delivery platform, *J. Am. Chem. Soc.* 132 (2010) 17227–17235.
- [46] G.T. Zugates, D.G. Anderson, S.R. Little, I.E.B. Lawhorn, R. Langer, Synthesis of poly(β -amino ester)s with thiol-reactive side chains for DNA delivery, *J. Am. Chem. Soc.* 128 (2006) 12726–12734.
- [47] A. Schädlich, H. Caysa, T. Mueller, F. Tenambergen, C. Rose, A. Göpferich, J. Kuntsche, K. Mäder, Tumor accumulation of NIR fluorescent PEG-PLA nanoparticles: Impact of particle size and human xenograft tumor model, *ACS Nano* 5 (2011) 8710–8720.
- [48] V. Filipe, A. Hawe, W. Jiskoot, Critical evaluation of nanoparticle tracking analysis (NTA) by Nanosight for the measurement of nanoparticles and protein aggregates, *Pharm. Res.* 27 (2010) 796–810.
- [49] C.D. Walkey, W.C.W. Chan, Understanding and controlling the interaction of nanomaterials with proteins in a physiological environment, *Chem. Soc. Rev.* 41 (2012) 2780–2799.
- [50] G.R. Dakwar, E. Zagato, J. Delanghe, S. Hobel, A. Aigner, H. Denys, K. Braeckmans, W. Ceelen, S.C. De Smedt, K. Remaut, Colloidal stability of nano-sized particles in the peritoneal fluid: towards optimizing drug delivery systems for intraperitoneal therapy, *Acta Biomater.* 10 (2014) 2965–2975.
- [51] H. Maeda, Tumor-selective delivery of macromolecular drugs via the EPR effect: background and future prospects, *Bioconjug. Chem.* 21 (2010) 797–802.
- [52] J. Fang, H. Nakamura, H. Maeda, The EPR effect: unique features of tumor blood vessels for drug delivery, factors involved, and limitations and augmentation of the effect, *Adv. Drug Deliv. Rev.* 63 (2011) 136–151.
- [53] T. Lammers, F. Kiessling, W.E. Hennink, G. Storm, Drug targeting to tumors: principles, pitfalls and (pre-) clinical progress, *J. Control. Release* 161 (2012) 175–187.
- [54] Y. Lee, K. Miyata, M. Oba, T. Ishii, S. Fukushima, M. Han, H. Koyama, N. Nishiyama, K. Kataoka, Charge-conversion ternary polyplex with endosome disruption moiety: a technique for efficient and safe gene delivery, *Angew. Chem. Int. Ed.* 47 (2008) 5163–5166.
- [55] S. Kunjachan, R. Pola, F. Gremse, B. Theek, J. Ehling, D. Moekel, B. Hermanns-Sachweh, M. Pechar, K. Ulbrich, W.E. Hennink, G. Storm, W. Lederle, F. Kiessling, T. Lammers, Passive versus active tumor targeting using RGD- and NGR-modified polymeric nanomedicines, *Nano Lett.* 14 (2014) 972–981.
- [56] F. Gremse, B. Theek, S. Kunjachan, W. Lederle, A. Pardo, S. Barth, T. Lammers, U. Naumann, F. Kiessling, Absorption reconstruction improves biodistribution assessment of fluorescent nanoprobes using hybrid fluorescence-mediated tomography, *Theranostics* 4 (2014) 960–971.
- [57] T. Merdan, K. Kunath, H. Petersen, U. Bakowsky, K.H. Voigt, J. Kopecek, T. Kissel, PEGylation of poly(ethylene imine) affects stability of complexes with plasmid DNA under *in vivo* conditions in a dose-dependent manner after intravenous injection into mice, *Bioconjug. Chem.* 16 (2005) 785–792.
- [58] Z. Ge, Q. Chen, K. Osada, X. Liu, T.A. Tockary, S. Uchida, A. Dirisala, T. Ishii, T. Nomoto, K. Toh, Y. Matsumoto, M. Oba, M.R. Kano, K. Itaka, K. Kataoka, Targeted gene delivery by polyplex micelles with crowded PEG palisade and cRGD moiety for systemic treatment of pancreatic tumors, *Biomaterials* 35 (2014) 3416–3426.
- [59] Y. Anraku, A. Kishimura, A. Kobayashi, M. Oba, K. Kataoka, Size-controlled long-circulating PICsomes as a ruler to measure critical cut-off disposition size into normal and tumor tissues, *Chem. Commun.* 47 (2011) 6054–6056.
- [60] N. Bertrand, J.-C. Leroux, The journey of a drug-carrier in the body: an anatomophysiological perspective, *J. Control. Release* 161 (2012) 152–163.
- [61] G. Storm, S.O. Belliot, T. Daemen, D.D. Lasic, Surface modification of nanoparticles to oppose uptake by the mononuclear phagocyte system, *Adv. Drug Deliv. Rev.* 17 (1995) 31–48.

- [62] A. Schädlich, C. Rose, J. Kuntsche, H. Caysa, T. Mueller, A. Göpferich, K. Mäder, How stealthy are PEG–PLA nanoparticles? An NIR *in vivo* study combined with detailed size measurements, *Pharm. Res.* 28 (2011) 1995–2007.
- [63] T. Nomoto, S. Fukushima, M. Kumagai, K. Machitani, Y. Matsumoto, Arnida, M. Oba, K. Miyata, K. Osada, N. Nishiyama, K. Kataoka, Three-layered polyplex micelle as a multifunctional nanocarrier platform for light-induced systemic gene transfer, *Nat. Commun.* 5 (2014).
- [64] U. Lächelt, P. Kos, F.M. Mickler, A. Herrmann, E.E. Salcher, W. Rödl, N. Badgular, C. Bräuchle, E. Wagner, Fine-tuning of proton sponges by precise diaminoethanes and histidines in pDNA polyplexes, *Nanomedicine* 10 (2013) 35–44.
- [65] C.H.J. Choi, J.E. Zuckerman, P. Webster, M.E. Davis, Targeting kidney mesangium by nanoparticles of defined size, *Proc. Natl. Acad. Sci. U. S. A.* 108 (2011) 6656–6661.
- [66] J.E. Zuckerman, C.H.J. Choi, H. Han, M.E. Davis, Polycation-siRNA nanoparticles can disassemble at the kidney glomerular basement membrane, *Proc. Natl. Acad. Sci. U. S. A.* 109 (2012) 3137–3142.
- [67] L. Brülisauer, G. Valentino, S. Morinaga, K. Cam, J. Thstrup Bukrinski, M.A. Gauthier, J.-C. Leroux, Bio-reduction of redox-sensitive albumin conjugates in FcRn-expressing cells, *Angew. Chem. Int. Ed. Engl.* 53 (2014) 8392–8396.
- [68] K.A. Mislick, J.D. Baldeschwieler, Evidence for the role of proteoglycans in cation-mediated gene transfer, *Proc. Natl. Acad. Sci. U. S. A.* 93 (1996) 12349–12354.
- [69] D. Vercauteren, J. Rejman, T.F. Martens, J. Demeester, S.C. De Smedt, K. Braeckmans, On the cellular processing of non-viral nanomedicines for nucleic acid delivery: mechanisms and methods, *J. Control. Release* 161 (2012) 566–581.
- [70] H.K. de Wolf, J. Luten, C.J. Snel, G. Storm, W.E. Hennink, Biodegradable, cationic methacrylamide-based polymers for gene delivery to ovarian cancer cells in mice, *Mol. Pharm.* 5 (2008) 349–357.
- [71] L. Wightman, R. Kircheis, V. Rössler, S. Carotta, R. Ruzicka, M. Kurs, E. Wagner, Different behavior of branched and linear polyethylenimine for gene delivery *in vitro* and *in vivo*, *J. Gene Med.* 3 (2001) 362–372.
- [72] J. Zhou, J. Liu, C.J. Cheng, T.R. Patel, C.E. Weller, J.M. Piepmeier, Z. Jiang, W.M. Saltzman, Biodegradable poly(amine-co-ester) terpolymers for targeted gene delivery, *Nat. Mater.* 11 (2012) 82–90.
- [73] Q. Yang, S.W. Jones, C.L. Parker, W.C. Zamboni, J.E. Bear, S.K. Lai, Evading immune cell uptake and clearance requires PEG grafting at densities substantially exceeding the minimum for brush conformation, *Mol. Pharm.* 11 (2014) 1250–1258.
- [74] T.A. Tockary, K. Osada, Q. Chen, K. Machitani, A. Dirisala, S. Uchida, T. Nomoto, K. Toh, Y. Matsumoto, K. Itaka, K. Nitta, K. Nagayama, K. Kataoka, Tethered PEG crowdedness determining shape and blood circulation profile of polyplex micelle gene carriers, *Macromolecules* 46 (2013) 6585–6592.
- [75] C.E. Nelson, J.R. Kintzing, A. Hanna, J.M. Shannon, M.K. Gupta, C.L. Duvall, Balancing cationic and hydrophobic content of PEGylated siRNA polyplexes enhances endosome escape, stability, blood circulation time, and bioactivity *in vivo*, *ACS Nano* 7 (2013) 8870–8880.